Nonthermal X-Ray Spectral Flattening Toward Low Energies in Early Impulsive Flares

Linhui Sui[1,2], Gordon D. Holman[2], and Brian R. Dennis[2]

ABSTRACT

The determination of the low-energy cutoff to nonthermal electron distributions is critical to the calculation of the nonthermal energy in solar flares. The most direct evidence for low-energy cutoffs is flattening of the power-law, nonthermal X-ray spectra at low energies. However, because of the plasma preheating often seen in flares, the thermal emissions at low energies may hide such spectral flattening of the nonthermal component. We select a category of flares, which we call "early impulsive flares", in which the > 25 keV hard X-ray (HXR) flux increase is delayed by less than 30 s after the flux increase at lower energies. Thus, the plasma preheating in these flares is minimal, so the nonthermal spectrum can be determined to lower energies than in flares with significant preheating. Out of a sample of 33 early impulsive flares observed by the *Ramaty High Energy Solar Spectroscopy Imager (RHESSI)*, nine showed spectral flattening toward low energies. In these events, the break energy of the double power-law fit to the HXR spectra lies in the range 10–50 keV, significantly lower than the value we have seen for other flares that do not show such early impulsive emissions. In particular, it correlates with the HXR flux. After correcting the spatially-integrated spectra for albedo from isotropically emitted X-rays and using *RHESSI* imaging spectroscopy to exclude the extended albedo halo, we find that albedo associated with isotropic or nearly isotropic electrons can only account for the spectral flattening in three flares near Sun center. The spectral flattening in the remaining six flares is found to be consistent with the existence of a low-energy cutoff in the electron spectrum, falling in the range 15-50 keV, which also correlates with the HXR flux.

Subject headings: Sun: flares—Sun: X-rays

---

[1]Department of Physics, The Catholic University of America, Washington, DC 20064.

[2]Solar Physics Laboratory, Code 671, NASA Goddard Space Flight Center, Greenbelt, MD 20771.

1. Introduction

One of the most remarkable aspects of solar flares is that a large fraction of the released energy is transferred to kinetic energy of electrons and ions (e.g., Emslie et al. 2004, 2005). Early observations have indicated that a considerable fraction of the flare energy (perhaps as high as 50%) is converted to accelerate electrons (Brown 1971; Lin & Hudson 1976) and ions (Ramaty et al. 1995). The evaluation of the energy partition in flares between thermal plasma and nonthermal electrons is hampered by observational limits. Although a thermal bremsstrahlung model with multiple temperatures can usually fit the data (Brown 1974; Emslie & Brown 1980; Brown & Emslie 1987), power-law photon spectra above ∼10 keV are generally understood to be produced by bremsstrahlung emission from nonthermal electrons that themselves have a power-law energy distribution. A low-energy cutoff is required to keep the total energy in electrons finite, given that electron distributions are steeper than E^{-2}, as determined from the measured hard X-ray (HXR) spectra assuming thin- or thick-target interactions (Dennis 1985; Lin & Schwartz 1987; Winglee et al. 1991; Holman et al. 2003). The total energy of the nonthermal electrons is very sensitive to the low-energy cutoff, particularly for flares with steep spectra. Uncertainties in the low-energy cutoff can lead to large uncertainties in the nonthermal energy. Most previous estimations of the total electron energy have been made with assumed (arbitrary) cutoff energies in the range of 20-30 keV (Dennis et al. 2003).

Even with the best flare spectra with ∼1 keV FWHM obtained with the *Ramaty High Energy Solar Spectroscopy Imager (RHESSI)*, the low-energy cutoff cannot be uniquely determined by spectral fitting alone. *RHESSI* spectra during the impulsive phase of a flare often show two components: a near-exponential (thermal) component at low energies and a flatter power-law or double power-law (nonthermal) component at higher energies. These two components merge smoothly together. Photon spectra produced by electron distributions with a range of cutoff energies up to a maximum value are able to fit the same X-ray spectrum equally well, because the nonthermal fluxes at low energies are usually much less than thermal fluxes. Therefore, only an upper limit on the low-energy cutoff can be obtained, giving a lower limit on the nonthermal electron energy (Holman et al. 2003). Recently, Sui et al. (2005) used a new method that combines spatial, spectral, and temporal analysis to determine the cutoff energy for a flare observed with *RHESSI*. A low-energy cutoff of 24±2 keV was obtained to ensure the thermal emission dominance over nonthermal emissions at low energies, smooth time profiles of plasma temperature and emission measure, and consistency between images and spectra for that event.

There has been debate on whether or not we need an abrupt low-energy cutoff to the nonthermal electron distribution. Emslie (2003) pointed out that nonthermal electrons with

energy $E \gtrsim kT$ (where k is Boltzmann's constant and T is the plasma temperature) lose energy at a rate significantly less than that in the cold target (E >> kT) that is usually assumed (e.g. Brown 1971). Moreover, electrons with $E \sim kT$ can even gain energy from the thermal plasma. Therefore, for these low-energy electrons, the target is warm and the total injected power from the nonthermal electrons should be determined by integrating only over energies $E \gtrsim kT$, giving a finite total nonthermal energy input. Emslie found that $5kT$ can be taken as an approximate low-energy cutoff. However, with $5kT$ as the cutoff energy, Holman et al. (2003) estimated the maximum nonthermal energy for the X4.8 flare on July 23, 2002, to be 4×10^{34} ergs, which is greater than the maximum total energy that has been deduced previously for even the largest solar flare. Furthermore, this warm-target argument cannot exclude the possibility of a low-energy cutoff that is higher than $5kT$. Therefore, it does not seem to be able to solve the low-energy cutoff issue.

The most direct evidence for low-energy cutoffs is spectral flattening of the power-law X-ray photon spectra at low energies. Nonthermal electrons with a low-energy cutoff produce a photon spectrum with a flattening at energies below the cutoff energy (e.g., Holman 2003). Therefore, if a low-energy cutoff does exist, the nonthermal part of flare spectra may flatten before disappearing under the thermal spectra at low energies. However, high-temperature thermal emission resulting from plasma heating before the particle acceleration usually prevents us from detecting this nonthermal flattening.

In order to search for evidence of low-energy cutoffs, we selected flares with little plasma preheating to avoid strong thermal emissions in the rise phase. We call such flares "early impulsive flares" (Sui et al. 2006a,b). In these early impulsive flares, the nonthermal spectra can be measured to lower energies than in flares with greater plasma preheating. Therefore, they offer us a better chance to detect any nonthermal spectral flattening due to the existence of low-energy cutoffs in the electron distributions.

The main purpose of this paper is to investigate whether the nonthermal, power-law spectra flatten at low energies in early impulsive flares. If so, can the spectral flattening be interpreted as evidence for the low-energy cutoff? The paper is organized as follows. In § 2 we describe how we search for early impulsive flares in the *RHESSI* flare catalog. In § 3 we present the spectral results of the selected early impulsive flares. Photospheric albedo correction to the spectra is made in § 4. The low-energy cutoff interpretation of the spectral flattening is described in § 5. A summary and discussion of our results, including possible interpretations, are in § 6.

2. Early Impulsive Flares

We searched the list of flares detected by *RHESSI* with the following two criteria: (1) the flares are detectable in the 25-50 keV band, i.e., the count rate increased in that band by $> 3\sigma$ above the background level, and (2) the 25-50 keV flux increased < 30 s after the start of the 12-25 keV flux increase. The first criterion enables us to select flares having significant nonthermal emission because the flux above 25 keV is usually dominated by nonthermal emission. The second criterion enables us to select flares with minimal plasma pre-heating. To limit the number of flares for this study, we searched for the early impulsive flares only from the *RHESSI* 2002 catalog.

From February 12, 2002, when *RHESSI* first became operational after launch, to the end of that year, 5308 flares were recorded by *RHESSI* with 610 detectable in the 25-50 keV band. Based on the two criteria stated above, we identified 160 flares as early impulsive flares. Therefore, we found that $\sim$25% of the flares detectable at >25 keV are early impulsive flares. To further reduce the number of the flares for spectral analysis in this study, we selected only those early impulsive flares with the peak 25-50 keV flux >3.5 times the background level of the same energy band. In the end, 33 flares were left for this study. Among the 33 flares, one flare is a *GOES* X-class flare, 8 are M-class flares, and 24 are C-class flares.

RHESSI light curves of four of the 33 early impulsive flares in this sample are shown in Figure 1. Except for the February 26, 2002, event, these flares had an impulsive HXR rise and a sharp HXR peak. It is evident that in each event the flux increase at high energies (>25 keV) started shortly after the start of the flare at lower energies. Because of the limited plasma preheating, the hard X-ray peaks in all four flares can also be seen at low energies down to the 6-12 keV band, indicating that the nonthermal emission contributes significantly to the low-energy flux. For example, this nonthermal peak is particularly evident as a shoulder in the 6-12 keV time profile of the April 22, 2002, flare (top left panel of Fig. 1).

3. Nonthermal Flattening in *RHESSI* Spectra

In order to check whether the spectra of the early impulsive flares show nonthermal flattening at low energies, we first investigate the spectra near the HXR peak time, when the nonthermal spectra are the strongest. We find in 9 out of the 33 flares we selected that the nonthermal part of the spectra flatten at low energies. In the following section, we present the detailed analysis of the flare that occurred on June 02, 2002.

3.1. June 02, 2002 flare

The June 02, 2002 flare is a *GOES* C9.4 flare that occurred near Sun center at [X:-150″, Y:300″]. Light curves are shown in Fig. 2. The flare had two HXR peaks. The first HXR peak has a corresponding peak in the 6-12 keV band, indicating nonthermal emission in that energy band very early in the flare. *RHESSI* images of this flare have been recently analyzed by Sui et al. (2006b) along with EUV and Hα observations. Besides a coronal source well above the height of the flare loops that developed later in the flare, the 6-12 keV images were dominated by two footpoints, indicating significant nonthermal contribution to this energy band early in the flare.

The *RHESSI* spectra, shown in Fig. 3, are also consistent with the nonthermal interpretation early in the flare. All the photon spectra are fitted to an iso-thermal spectrum at low energies and a nonthermal, double power-law spectrum at high energies. The thermal spectrum includes both continuum and line emissions as derived using CHIANTI (v. 5.2) (Landi et al. 2006) with coronal abundances and Mazzotta et al. (1998) ionization fractions. The major atomic line complexes seen by *RHESSI* below 10 keV are the iron line complex at ∼6.7 and the iron/nickel line complex at ∼8 keV (Phillips 2004). As shown in the spectrum very early in the flare (Fig. 3a), the thermal and nonthermal fluxes contribute almost equally at ∼8 keV. The nonthermal emission continued to contribute significantly to the fluxes below 10 keV until the time of the first HXR peak (Fig. 3c). This is consistent with the light curve during the same period, which shows that the nonthermal >25 keV HXR peak extended to the 6-12 keV band. It is also consistent with the *RHESSI* images showing two footpoints in the 6-12 keV band early in the flare. After the first HXR peak, the spectra at energies below 12 keV are dominated by thermal emission, in agreement with the smoother light curve at 6-12 keV.

Also shown in Fig. 3 and all subsequent spectral fits are the normalized residuals. A normalized residual is the ratio of the difference between the observed flux and the model flux to the one-sigma uncertainty in the observed flux. These, along with the minimum value of the chi-squared obtained from the fit, indicate the quality of the fit.

The spectral fits indicate that the break energy of the double power-law spectra varied with time and was in general correlated with the HXR flux (Figure 4). For the spectrum at 11:44:12–11:44:16 UT (Fig.3a, hereafter only the start time of each 4 s time interval is stated), the 10 keV break energy can only be considered as an upper limit because any break energy below that value can fit the spectrum equally well. After 8 s when the HXR flux had risen significantly, the break energy increased to ∼21 keV (Fig. 3b). The break energy continued to increase and reached 27 keV at the first HXR peak (Fig. 3c). As the HXR flux decreased, the break energy also decreased. It dropped to ∼18 keV when the HXR flux

reached its lowest level after the first peak (Fig. 3d). After that, the break energy increased again when the HXR flux increased, reaching ∼26 keV ∼4 s before the second HXR peak (Fig. 3e). However, at the time of the second HXR peak (11:44:52 UT) (Fig. 3f), the break energy had decreased to $\lesssim$20 keV. In fact, the nonthermal spectrum at this time can be fitted well to a single power-law function. The 20 keV value is just an upper limit to the break energy, as for the very early spectrum shown in Figure 3a. The break energy of the spectra after the second HXR peak continued to decrease down to $\lesssim$15 keV at later times.

The time evolution of the break energy obtained during the impulsive part of the flare is shown in Figure 4b (*dashed line*). Ranging from $\lesssim$10 to 27 keV, it correlates with the HXR flux. The Spearman's rank correlation coefficient, calculated using the IDL function "r_correlate.pro", is 0.83. We calculate the rank correlation coefficient instead of the more commonly used Pearson's linear correlation coefficient because it does not assume a linear relationship. The probability of obtaining this correlation coefficient by chance is less than 0.002%. This correlation is most evident during the first HXR peak.

3.2. Remaining Early Impulsive Flares

The 9 flares identified to show low-energy spectral flattening are listed in Table 1. All but the M2.6 flare are *GOES* C-class flares. Three flares (# 1, 2 and 9) occurred within 14° of the solar limb. Spectral fitting indicates that the break energy varies with time for all the events. For all the events, early in the flare the nonthermal part of the spectra have a single power-law distribution, which extends down to very low (<10 keV) energies (e.g., Fig. 3a). As the flares progress, a double power-law model is needed to fit the nonthermal spectrum. The deduced break energy mostly ranges between <10 and 40 keV, with two flares (# 2 and 8) giving values above 40 keV, which is much lower than the typical break energy for commonly seen broken power-law spectra (e.g. Dulk et al. 1992; Gan et al. 2002a). The correlation between the break-energy and HXR flux can be seen in all 9 flares, with the correlation coefficient ranging from 0.6 to 0.85.

4. Photospheric Albedo and Its Contribution to Flare Spectra

4.1. Photospheric Albedo

Photospheric albedo can distort the primary flare spectra significantly. Flare-produced photons are emitted both upward (toward the observer) and downward (toward the photosphere). The downward-emitting photons in the energy range 10-100 keV have a high

probability of being reflected back due to Compton scattering with electrons in the photosphere, with the spectral reflectivity peaking around 30 keV (Bai & Ramaty 1978). The contribution of the albedo flux depends on flare location, source height, photon emission anisotropy, and power-law spectral index. The closer the flare is to Sun center and the harder the photon spectrum, the stronger the albedo relative to the direct emission.

Photospheric albedo can cause spectral flattening at low energies, similar to the flattening caused by a low-energy cutoff to the nonthermal electron distribution. Zhang & Huang (2004) compared the spectra flattening caused by both the albedo effect and a low-energy cutoff to the electron distribution. They found that, for harder spectra (photon power-law index $\gamma < 3$), the albedo-caused flattening is comparable to or larger than that caused by the low-energy cutoff. For softer spectra ($\gamma > 3$), the albedo-caused flattening is smaller, consistent with the results of Alexander & Brown (2002). The joint contributions of the albedo effect and a low-energy cutoff will result in more flattened spectra than caused by either effect alone. However, distinguishing between these two factors is not easy. Recently, Kontar et al. (2006) developed an albedo correction method using an angle-dependent Green's function approach.

Because the break-energy we obtained for the 9 early impulsive flares is mostly around 30 keV (see Table 1), near the reflectivity peak of albedo flux, we first investigate the albedo contribution in these flares.

4.2. Albedo Correction to *RHESSI* spectra

To correct for the albedo contamination, we use the albedo correction routine used by Kontar et al. (2006) and Kasparova et al. (2007), which has been incorporated into the *RHESSI* spectral analysis software. Because of electron pitch-angle scattering, the emitted hard X-rays are assumed to be isotropic as was assumed by Kontar et al. (2006) and Kasparova et al. (2007). Recently, Kontar & Brown (2006) derived a new technique to obtain the downward- and upward-directed electron distributions simultaneously using *RHESSI* spectral data. They found that electrons are near-isotropic for the two flares they analyzed, in contradiction to the standard collisional thick-target model which assumes a purely downward-directed electron beam (Brown 1971).

After the albedo correction, we find that the nonthermal flattening is eliminated almost completely in flares 6, 7 and 8. For these three flares, the originally required double power-law function is not needed to fit the nonthermal part of the spectrum. Instead, a single power-law function is sufficient to fit the albedo-corrected spectrum in each case. Figure 5

shows the spectra at the HXR peak of the September 29, 2002, flare (flare 8) before (left panel) and after (right panel) albedo correction. The normalized residuals are also plotted below each spectrum. As expected, the thermal part of the spectrum does not significantly change before and after the albedo correction, because the albedo flux mainly contaminates the spectrum in the range between 10 and 100 keV. The nonthermal parts of the spectra around 30 keV do change significantly. Before the albedo correction, the nonthermal part of the spectrum is fitted to a double power-law spectrum with acceptable residuals. After the albedo correction, it can be fitted to a single power-law spectrum (right panel). A break energy of ∼20 keV is needed to make a smooth transition from the nonthermal to the thermal spectrum. We note that although a single power-law function gives an acceptable value of χ^2 for the nonthermal spectrum above 20 keV, the systematically varying residuals between 20 and 60 keV suggest a deviation from the model. This could mean that either the albedo component has not been completely eliminated or other mechanisms may also contribute to the flattening.

For the other flares (# 1 to 5 and 9), after the albedo correction the nonthermal part of the spectra cannot be fitted to a single power-law function with acceptable χ^2 and residuals. They still require a double power-law function. Figure 6 shows an albedo-corrected spectrum at the HXR peak of the June 2, 2002, flare. The spectrum without the albedo correction is shown in Fig. 3c. The albedo-corrected spectrum is fitted to a single power-law function above ∼21 keV (left panel) and to a double (right panel) power-law function. It is evident that the double power-law fit is better than the single power-law fit, because (1) the residuals of the single power-law fit indicate a deviation from the model between 20 and 70 keV, and (2) the reduced χ^2 of 1.4 for the single power-law fit is significantly larger than the 1.0 value for the double power-law fit. The break energies obtained from the albedo-corrected spectra (Fig. 4b, *dotted lines*) still correlate with the HXR flux. Moreover, they are mostly larger than the break energies obtained for the spectra not corrected for albedo.

Like the June 2 flare, the nonthermal parts of the albedo-corrected spectra of the other 5 flares also require a double power-law fit. The break energies obtained from the albedo-corrected spectra still correlate with the HXR flux in all these events. The break energies are higher than those obtained before the albedo correction.

4.3. Albedo Test with *RHESSI* Imaging Spectroscopy

Because the albedo emission is produced by scattering of the original HXRs, the albedo source size should be larger than the primary sources. Schmahl & Hurford (2002) identified the presence of "halo" sources in *RHESSI* images with size scales larger than the flare "core"

by a factor of 3–7, and suggested that they could be albedo sources.

We can reduce the albedo contribution by summing the flux only from the primary flare region within the *RHESSI* images. We then check the power-law flattening in the nonthermal spectrum of the primary flare. If the flattening is seen in the spatially-integrated spectrum, but cannot be seen in the spectrum of the primary source, it is likely that the nonthermal flattening results from the albedo contribution. On the other hand, if the nonthermal flattening can be seen in both the spatially-integrated spectrum and the spectrum of the primary source, then the spectral flattening may not be caused by the albedo contribution. *RHESSI* imaging spectroscopy offers a way to test this hypothesis.

To obtain the spectra of the primary flare sources, we first made *RHESSI* images in multiple energy bands during a time period when the nonthermal flattening is evident in the spatially-integrated flare spectra. We then picked an appropriate contour level (say, 20% or 30% of the peak flux, depending on the specific image) so as to include only the flux from the core flare source(s) in each image. The spectrum of the primary source can be obtained by summing the flux above this contour level in each image. Using the same method as used in fitting the spatially-integrated spectrum, we determine the best spectral fitting model, i.e., single versus double power-law function.

The fitting of the imaged spectra of the primary flare sources confirms that albedo caused the spectral flattening in the spatially integrated spectra in flares 6, 7 and 8. The nonthermal spectrum of the primary flare sources in these three flares can be fitted to a single power-law function. This is in agreement with the earlier results obtained with the albedo correction. For the other 6 flares, however, the nonthermal spectra of the primary sources still flatten at low energies and require a double power-law fit. Two examples are shown in Figure 7. The primary source spectrum of the September 29 flare (flare 8) can be well fitted to a single power-law function (left panel). It is evident that the fluxes of the spatially integrated spectrum without albedo correction (gray solid line) are higher than the primary source spectrum (dark solid line). The greatest difference lies near 30 keV, where the albedo flux contributes the most. Moreover, the fluxes of the albedo-corrected spectrum (gray dashed lines) are very close to the primary source at all energies above 15 keV where the nonthermal flux dominated, confirming that albedo is a major cause of the nonthermal flattening in this event. In contrast, the primary source spectrum of the June 02, 2002, flare (Figure 7, right panel) still shows nonthermal flattening, which requires a double power-fit fit with a break energy at $\sim$23 keV. Also unlike the September 29 flare, the spectrum without the albedo correction differs from the primary source spectrum mostly between 10 and 20 keV. The primary source spectrum is still different from the albedo-corrected spectrum (gray dashed line), which has a double power-law distribution with a

break at 42 keV. At this moment, we do not know how to explain the difference between the primary source spectrum and albedo-corrected spectrum.

5. Low-Energy Cutoff Interpretation

Based on the discussion above, the nonthermal spectral flattening in the remaining 6 flares is not likely to be entirely due to albedo. We now want to check whether the spectral flattening can be interpreted as the result of a low-energy cutoff in the nonthermal electron distribution, which is the major motivation of this study.

In order to check whether the spectral flattening can be interpreted as evidence for the low-energy cutoffs, we first apply the albedo correction as developed by Kontar et al. (2006) to the *RHESSI* spatially-integrated photon spectra, then fit the nonthermal part of the spectrum to a thick-target bremsstrahlung spectrum produced by electrons that have a power-law distribution and a low-energy cutoff. We find that the nonthermal part of the spectra in all 6 flares can be well fitted to this model, showing that the existence of a low-energy cutoff is a possible explanation for the flattening in the nonthermal photon spectra. Figure 8 shows two spectra of the June 2, 2002, flare fitted with such a model. The deduced cutoff energies are 28 and 38 keV, respectively. The deduced low-energy cutoff also correlates with the HXR flux. The low-energy cutoffs obtained for the June 02 flare are shown in Figure 4c.

The range of the low-energy cutoffs for all 6 flares are listed in Table 1. The cutoff energies for flares 4 and 5 vary between ∼20 and 30 keV, close to the values of 20 keV usually assumed (Dennis et al. 2003, and reference therein). For the rest of the flares, although the lower limit of the cutoff range is ∼20 keV, the upper limit of ∼40 keV (even 49 keV for the June 2, 2002, flare) is higher than often assumed.

6. Summary and Discussions

In order to find evidence for the low-energy cutoff to the nonthermal electron distribution, we searched for spectral flattening in HXR spectra at energies between ∼10 and ∼50 keV. For this purpose, we selected flares, which we call "early impulsive flares," where the impulsive, nonthermal hard (>25 keV) X-ray flux rises very early in the flare as compared to the rise of the soft X-ray emission. Due to the absence of intense plasma preheating to ∼10 MK in these early impulsive flares, the thermal emission is weak early in these flares relative to the nonthermal emission. Consequently, the nonthermal part of the X-ray spec-

trum can be detected to much lower energies than in flares with stronger plasma preheating. For this study, we selected 33 early impulsive flares observed with *RHESSI* in 2002 that have substantial emissions above 25 keV. We found 9 flares showing evident spectral flattening at low energies (Table 1).

We found that the nonthermal HXR spectrum evolved significantly during the course of all 9 flares. Early in the flares, the nonthermal component of the spectra was consistent with a single power-law distribution above the isothermal component (see Fig. 3a). As the flares progressed and the HXR flux increased with time, the nonthermal spectra evolved to a double power-law form. After the HXR impulsive peaks, the double power-law spectra evolved back to a single power-law form.

The double power-law, nonthermal spectra of these early impulsive flares are different from commonly seen double power-law flare spectra. First, compared to the typical break energy (∼60–100 keV, e.g., Kane & Anderson 1970; Dulk et al. 1992), the break energies of these early impulsive flares (∼10-50 keV) are typically much lower. Most of the flares studied here could not be detected much above ∼50 keV, so no information is available on possible spectral breaks at higher energies. Second, the break energy in the early impulsive flares varies with time and correlates with the HXR flux. Dulk et al. (1992) did a statistical analysis of 93 flares observed by the Hard X-Ray Burst Spectrometer on the *Solar Maximum Mission (SMM)*, and did not find any correlation between the break energy and the HXR flux. Recent spectral analysis with *RHESSI* did not show any correlation either (e.g., Holman et al. 2003). Therefore, the double power-law spectra we found in the early impulsive flares could be caused by a different mechanism than the one responsible for the previously reported double power-law spectra.

We have checked to determine if the albedo flux can fully account for the nonthermal flattening. We applied the (isotropic) albedo correction routine recently developed by Kontar et al. (2006) to the spatially integrated flare spectra, and found that it can eliminate the nonthermal flattening in three flares (see Fig. 5) that occurred near Sun center. This result is in agreement with the recent findings of Kasparova et al. (2007) which indicate that low-energy cutoffs sometimes inferred for mean electron spectra are albedo artifacts. For the remaining 6 flares (4 flares near the solar limb and 2 flares near Sun center), albedo-corrected spectra still show significant flattening and require a double power-law fit (Fig. 6).

To further check the credibility of the albedo correction results, we obtained the spectra of the primary sources (or "core sources" as they were called by Schmahl & Hurford (2002)) using *RHESSI* imaging spectroscopy. This technique works because the albedo source is larger than its corresponding primary source. We find that the primary source spectra do not show the nonthermal flattening for the three flares whose nonthermal flattening can

be accounted for by the albedo flux (Fig. 7a). For the other 6 flares whose nonthermal flattening remains in the albedo-corrected spectra, the primary source spectra also show the nonthermal flattening (Fig. 7b). Moreover, because the albedo correction was applied assuming an isotropic photon distribution, its agreement with the imaging spectroscopy results suggests that the photons of the primary sources were indeed emitted isotropically by an isotropic electron distribution, supporting the recent results of Kontar & Brown (2006) obtained using a different approach.

The assumption of an isotropic electron distribution is, nevertheless, a lower-limit estimation of the albedo contribution. If we assume that the electron distribution is anisotropic, in order to fully account for the nonthermal flattening, the ratio of downward- to upward-directed electrons needs to be $\sim$3 for the June 2, 2002 flare. In other words, the nonthermal electrons are mostly downward-directed. On the other hand, among the 6 flares in which nonthermal flattening remains, 4 of them are limb flares. The albedo contribution in these four flares should not be significant, even allowing for an anisotropic source distribution. Therefore, albedo is unlikely to explain all the nonthermal flattening we find in these early impulsive flares close to the limb.

Electron distributions with low-energy cutoffs offer an explanation for the nonthermal flattening. We find that all the albedo-corrected spectra can be fitted to thick-target bremsstrahlung spectra produced by injected electrons with a low-energy cutoff to their power-law distributions (Fig. 8). Similar spectral flattening may have been observed by Nitta, Dennis, & Kiplinger (1990) in two flares seen by *SMM* and *Hinotori* with relatively poor-resolution spectrometers. Nitta, Dennis, & Kiplinger (1990) claimed that the spectral flattening seen in those two flares indicated a cutoff energy of $\gtrsim$50 keV. The light curves of the two flares they analyzed showed "short but intense" HXR fluxes with "relatively weak soft X-ray emissions," like the early impulsive flares we define in this paper. Therefore, it is not surprising for them to have discovered similar spectral flattening in those two events.

The deduced low-energy cutoff is found to correlate with the HXR flux. Because the HXR flux is an indicator of the efficiency of particle acceleration, this correlation could suggest that more efficient particle acceleration results in a higher low-energy cutoff and therefore a larger average electron energy. The evolution of the low-energy cutoff was explored by Gan et al. (2002b) with BATSE/*CGRO* data. Because of the limited energy coverage and spectral resolution of the BATSE/*CGRO*, they selected 3 events with break energies greater than 45 keV for their study. They found that the low-energy cutoff changed with time from 60 to 90 keV and generally correlated with the HXR flux. In a recent study of the "Neupert Effect" by Veronig et al. (2005), assuming that the electron beam heating is the main cause of the plasma heating in flares, they found that the low-energy cutoff needs

to vary with time in order to match the nonthermal energy carried by electron beams with the thermal energy required for heating the soft X-ray emitting plasma. However, no obvious correlation between the low-energy cutoff and the HXR flux was detected in the four flares they studied.

We note that, because of the soft-hard-soft (SHS) spectral evolution (e.g., Grigis & Benz 2004, and references therein), the correlation between the low-energy cutoff and the HXR flux does not have to result in an anti-correlation between nonthermal energy flux and the HXR flux. The SHS HXR spectral evolution results from SHS electron spectral evolution. When the low-energy cutoff increases, and the electron spectra harden with time and extend to higher energies, the total energy in electrons could still increase with time before the HXR peak. When the low-energy cutoff decreases and the electron spectra soften with time after the HXR peak, the nonthermal electron energy could decrease if the spectral softening counteracts the cutoff energy decrease. As shown in Fig. 4d, in the June 02, 2002, flare, in particular during the first HXR peak, both the cutoff energy and the nonthermal energy correlate in a general way with the HXR flux. However, in this case, the low energy electron cutoff energy peaks ∼4 s before the HXR peak and the total energy in electrons peaks 8–12 s later.

Although the often assumed sharp low-energy cutoff model, (i.e., no nonthermal electrons below the cutoff) is used in the spectral fitting, the spectra can be fitted equally well with a flat-cutoff model, for example, with a constant electron number distribution below the cutoff. With the *RHESSI* data alone, we cannot distinguish between the two cutoff models, which is in agreement with the results of Saint-Hilaire & Benz (2005). The results of the flat-cutoff model are very close to those derived from the sharp-cutoff model. Saint-Hilaire & Benz found that the nonthermal energies do not differ significantly for these two cutoff models, with the flat cutoff model (or "turnover" model in their paper) offering ∼20%–25% more energy. The sharp-cutoff model is physically unstable and leads to plasma instability (e.g., Saint-Hilaire & Benz 2005). Thus the sharp cutoff model is simply a convenient approximation to the unknown spectral dependence below the cutoff energy.

A possible explanation for the nonthermal flattening, other than a low-energy cutoff in the electron distribution injected from the acceleration region, is the effect of a return current (Zharkova & Gordovskyy 2006, and reference therein). The steady injection of nonthermal electrons into flare loops is expected to induce an electric field that results in a co-spatial return current carried by electrons in the plasma. The induced electric field also decelerates the precipitating electrons. Due to the combined effect of the self-induced electric field and Coulomb collisions, the nonthermal electrons with lower energies (<100 keV) can lose significant energy during their propagation, resulting in the loss of lower-energy electrons

in the upper atmosphere. The differential nonthermal electron distribution can peak at 40-80 keV, depending on the strength of the beam flux (Zharkova & Gordovskyy 2006). Because the relative energy loss suffered by the injected electrons is greatest for the lower energy particles, the new electron distribution flattens at low energies, resulting in the flattening of the spatially-integrated photon spectrum. Zharkova & Gordovskyy (2006) show that the more intense the beam flux, the higher the "break" energy, consistent with the correlation between the HXR flux and break energy we found in this study. Other phenomena that need to be considered in a more detailed analysis of these HXR spectral results are the possible effects of free-bound emissions (Brown and Mallik 2007) and nonuniform target ionization (Kontar et al. 2002). In future studies, we plan to include these effects in the analysis and test the return current model with the *RHESSI* spectral data presented in this paper.

We thank Edward Kontar and Jana Kasparova for their valuable discussions and suggestions, and Goddard summer student Ryan Hamilton for help in producing some of the figures. The work is supported by the *RHESSI* project and NASA grant NNX06AE64G. CHIANTI is a collaborative project involving NRL (USA), RAL (UK), and the following Universities: College London (UK), of Cambridge (UK), George Mason (USA), and of Florence (Italy).

REFERENCES

Alexander, R. C., Brown, J. C. 2002, Sol. Phys., 210, 407

Bai, T., Ramaty, R. 1978, ApJ, 219, 705

Brown, J. C. 1971, Sol. Phys., 18, 489

Brown, J. C., in Jr G. A. Newkirk (ed), Coronal Disturbances, IAU Symp. 1974, 57: 105

Brown, J. C., & Emslie, A. G. 1987, Sol. Phys., 110, 305

Brown, J. C. and Mallik, P. C. V. 2007, arXiv:0706.2823v1 [astro-ph], A&AS, submitted.

Dennis, B. R. 1985, Sol. Phys., 100, 465

Dennis, B. R., Veronig, A., Schwartz, R. A., Sui, L., Tolbert, A. K., Zarro, D. M., and the *RHESSI* Team 2003, Adv. Space Res., Vol. 32, No. 12, 2459

Dulk, G. A., Kiplinger, A. L., Winglee, R. M. 1992, ApJ, 389, 756

Emslie, A. G., & Brown, J. C., 1980, ApJ, 237, 1015

Emslie, A. G. 2003, ApJ, 595, L119

Emslie, A. G., Kucharek, H., Dennis, B. R., Gopalswamy, N., Holman, G. D., Share, G. H., Vourlidas, A., Forbes, T. G., Gallagher, P. T., Mason, G. M., Metcalf, T. R., Mewaldt, R. A., Murphy, R. J., Schwartz, R. A., and Zurbuchen, T. H. 2004, J. Geophys. Res., 109, 10104

Emslie, A. G., Dennis, B. R., Holman, G. D., and Hudson, H. S. 2005, J. Geophys. Res., 110, 11103

Gan, W., Li, Y., Chang, J., McTiernan, J. M., 2002a, Sol. Phys., 207, 137

Gan, W., Li, Y., Chang, J., 2002b, Chinese J. of Astronomy & Astrophysics, 2, 103

Grigis, P. C., & Benz, A. O. 2004, A&A, 426, 1093

Holman, G. D. 2003, ApJ, 586, 606

Holman, G. D., Sui, L., Schwartz, R. A., Emslie, A. G. 2003, ApJ, 595, L97

Kane, S. R., & Anderson, K. A. 1970, ApJ, 162, 1003

Kasparova, J., Kontar, E. P., & Brown, J. C. 2007, A&A, 466, 705

Kontar, E. P., Brown, J. C. & McArthur, G. K., 2002, Sol. Phys., 210, 419

Kontar, E. P., MacKinnon, A. L., Schwartz, R. A., Brown, J. C. 2006, A&A, 446, 1157

Kontar, E. P., Brown, J. C. 2006, ApJ, 653, L149

Landi, E., Del Zanna, G., Young, P.R., Dere, K.P., Mason, H.E., and Landini, M., 2006, ApJS, 162, 261

Lin, R. P., & Hudson, H. S. 1976, Sol. Phys., 50, 153

Lin, R. P., & Schwartz, R. A. 1987, ApJ, 312, 462

Mazzotta, P., Mazzitelli, G., Colafrancesco, S., & Vittorio, N. 1998, A&AS, 133, 403

Nitta, N., Dennis, B. R., & Kiplinger, A. L. 1990, ApJ, 353, 313

Phillips, K. J. H. 2004, ApJ, 605, 921

Ramaty, R., Mandzhavidze, N., Kozlovsky, B., and Murphy, R. J. 1995, ApJ, 455, L193

Saint-Hilaire, P., & Benz, A. O. 2005, A&A, 435, 743

Schmahl, E. J., &Hurford, G. J. 2002, Sol. Phys., 210, 273

Sui, L., Holman, G. D., & Dennis, B. R. 2005, ApJ, 626, 1102

Sui, L., Holman, G. D., & Dennis, B. R. 2006a, ApJ, 645, L157

Sui, L., Holman, G. D., & Dennis, B. R. 2006b, ApJ, 646, 605

Veronig, A. M., Brown, J. C., Dennis, B. R., Schwartz, R. A., Sui, L., Tolbert, A. K. 2005, ApJ, 621, 482

Winglee, R. M., Kiplinger, A. L., Zarro, D. M., Dulk, G. A., & Lemen, J. R. 1991, ApJ, 375, 366

Zhang, J., Huang, G. L. 2004, Sol. Phys., 219, 135

Zharkova, V. V., Gordovskyy, M. 2006, ApJ, 651, 553

Table 1. *RHESSI* 2002 early impulsive flares with spectral flattening.

Flare Index	Date of 2002	Peak Time UT	Flare Class	Helio. Angle (deg.)	Rank Correl. Coeff. of E_b and HXR	E_b without albedo (keV)	E_b with albedo (keV)	E_{cutoff} (keV)	albedo causes spectral flattening
1	Feb 25	21:27	C4.1	76	0.85	8–40	11–52	20–49	unlikely
2	Feb 26	10:27	C9.6	84	0.60	12–43	16–43	27–42	unlikely
3	Jun 02	11:46	C9.4	21	0.83	10–27	16–37	18–38	unlikely
4	Aug 21	17:22	C4.8	71	0.82	16–34	21–34	20–29	unlikely
5	Sep 02	21:27	C2.0	32	0.71	18–29	18–37	14–33	unlikely
6	Sep 14	00:08	C1.2	14	0.84	9–27	N/A	N/A	likely
7	Sep 17	04:23	C1.2	34	0.82	10–31	N/A	N/A	likely
8	Sep 29	06:38	M2.6	19	0.75	20–47	N/A	N/A	likely
9	Nov 14	11:10	C5.5	80	0.85	17–37	15–37	18-40	unlikely

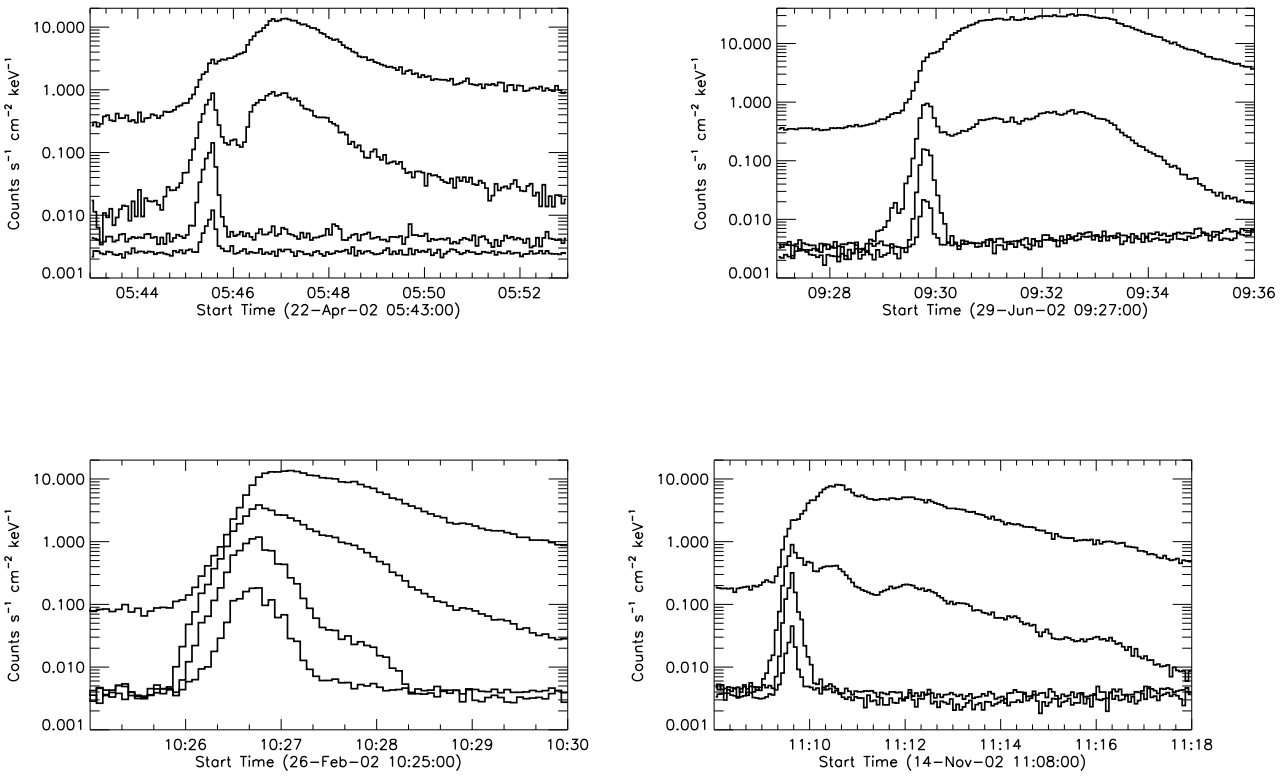

Fig. 1.— *RHESSI* count-rate light curves for four early impulsive flares. In each panel, the four energy bands from top to bottom are 6–12, 12–25, 25–50, and 50–100 keV, respectively. The time resolution is 4 s. The attenuator state for all the flares was A1, except for the 2002 June 29 flare with attenuator state A0.

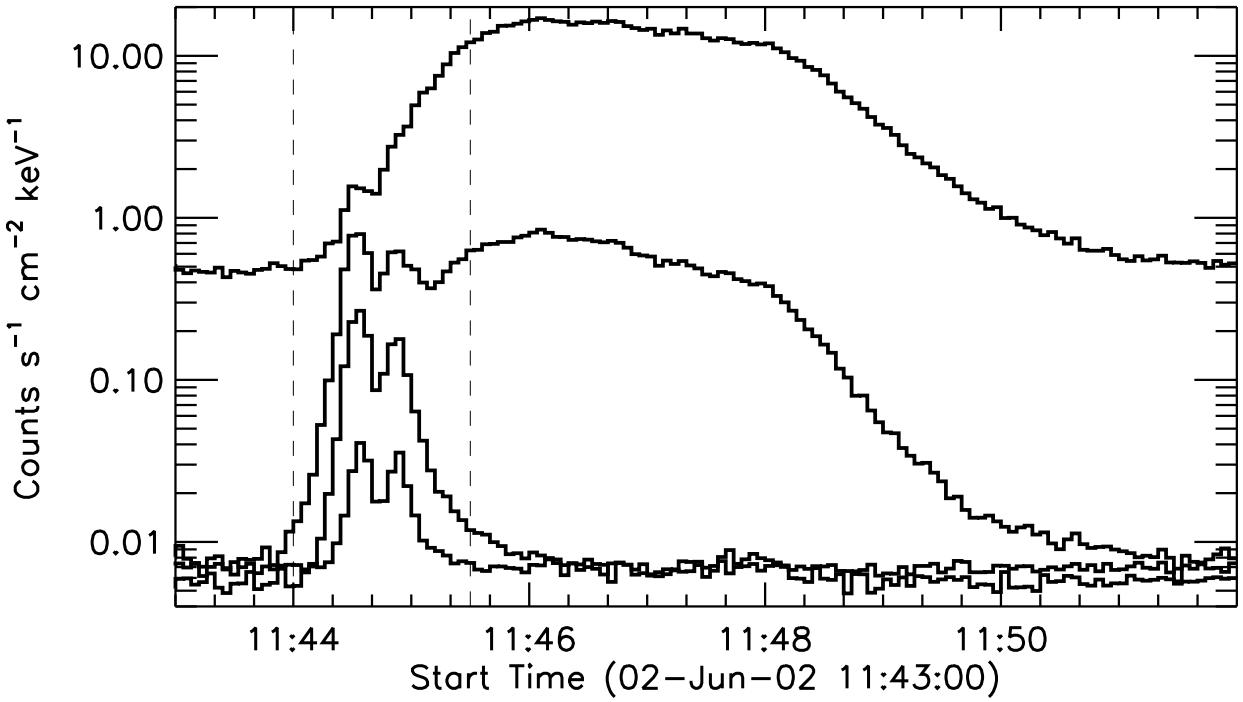

Fig. 2.— *RHESSI* light curves of the flare on June 02, 2002, with 4 s time bins. The four energy bands from top to bottom are 6–12, 12–25, 25–50, and 50–100 keV, respectively. The two dashed vertical lines indicate the time range of Fig. 4.

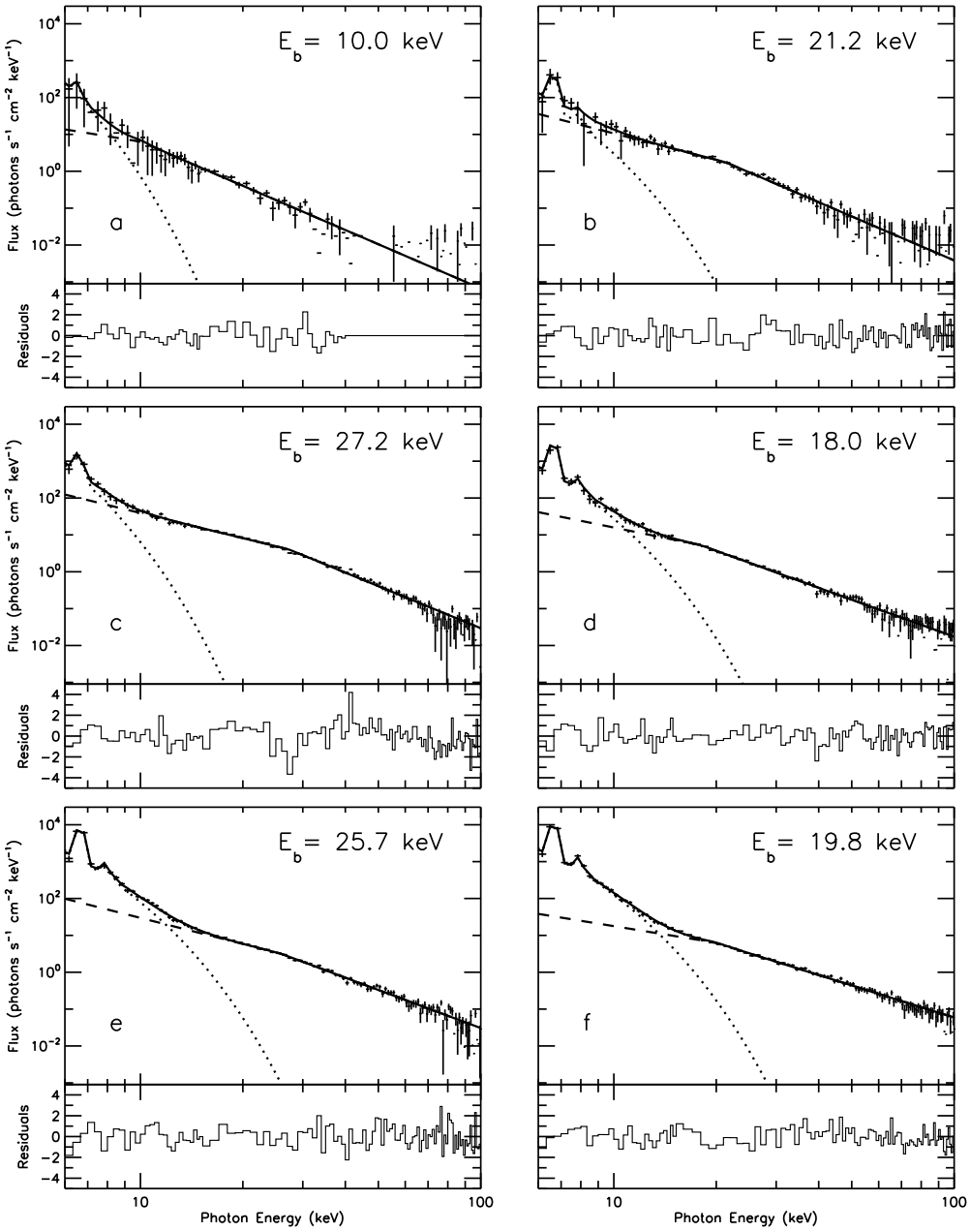

Fig. 3.— *RHESSI* spectra of the flare on June 02, 2002. The integration time of each spectrum is 4 s. The start and end times of each time interval are indicated in Fig. 4a. Each spectrum is fitted with a model consisting of an isothermal bremsstrahlung component (dotted line) and a nonthermal, double power-law component. The break energy E_b is indicated for each spectrum. The normalized residuals of the fits, defined as the observed flux minus the model flux divided by the estimated 1σ uncertainty in each data point, are also shown below each spectrum. The instrumental systematic uncertainty is set to zero for the fits in this paper.

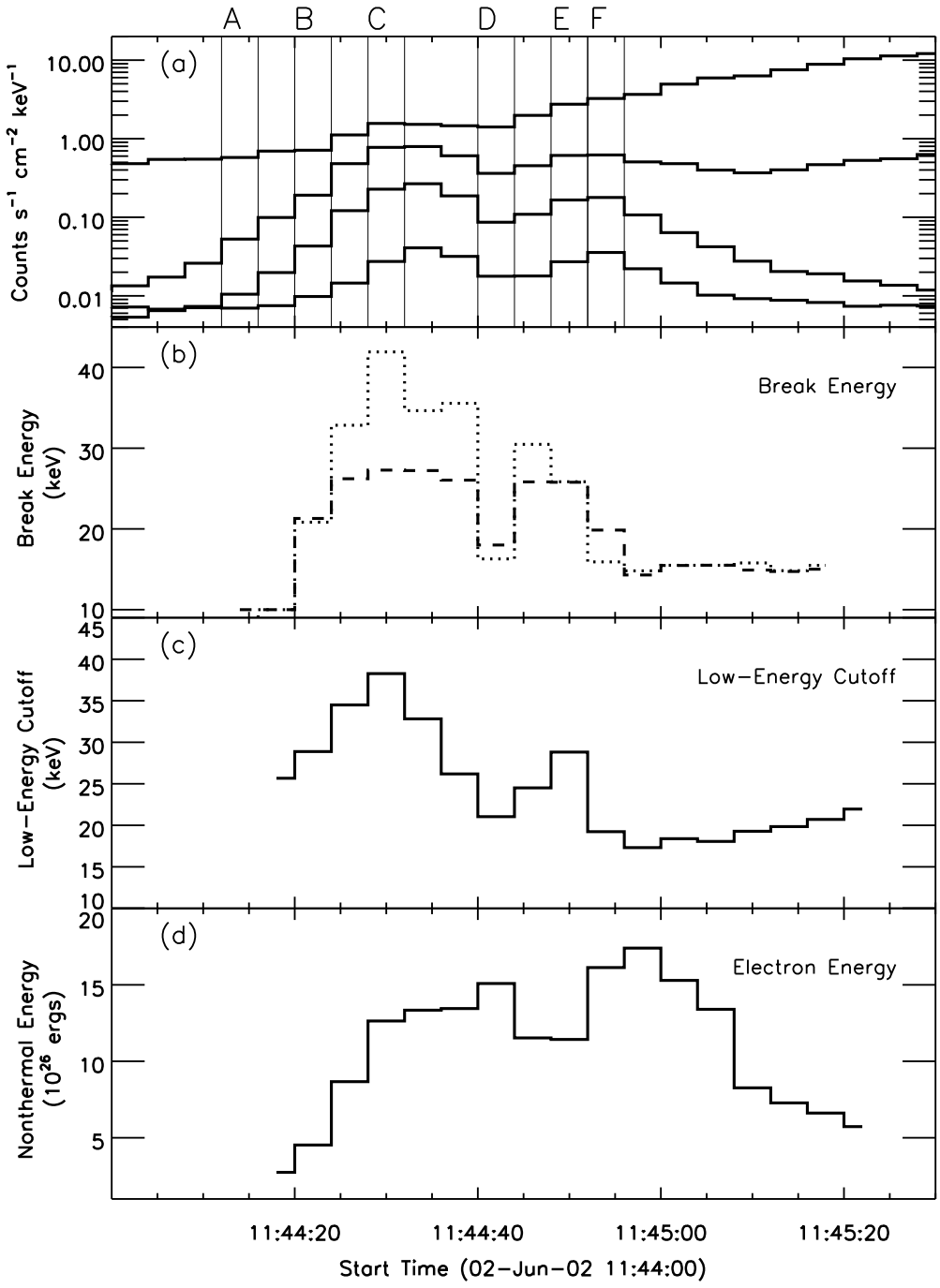

Fig. 4.— Panel a: Early part of the light curve shown in Fig. 2. The vertical, solid lines indicate the start and end times of each interval for the spectra shown in Fig. 3. Panel b: the break energy in the photon spectrum before (dashed line) and after (dotted line) the albedo correction. Panel c: low-energy cutoff to the power-law, nonthermal electron distribution. Panel d: the nonthermal electron energy in each 4 s time interval computed using the derived low-energy cutoff for each time interval.

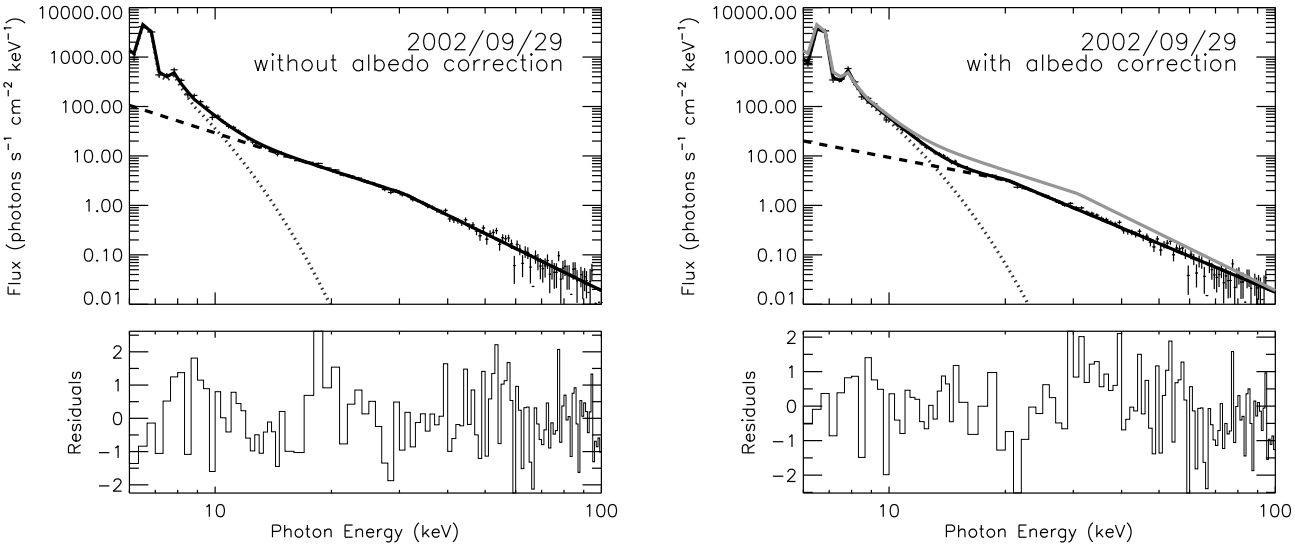

Fig. 5.— *RHESSI* spectrum at the HXR peak (06:35:28-06:35:32 UT) of the September 29, 2002 flare. Left Panel: spectrum without albedo correction. The nonthermal part is fitted to a double power-law model with a break energy of 30 keV. Right panel: spectrum with albedo correction (dark, solid line) and without albedo correction (gray, solid line, the same as the left panel). The nonthermal part of the albedo-corrected spectrum is fitted to a single power-law spectrum above 20 keV. A break energy at 20 keV is needed to make a smooth transition from the nonthermal to the thermal spectrum. The normalized χ^2 value of the fits in the left and right panels are 1.01 and 1.03, respectively. The plots in the bottom row show the normalized residuals of the fits.

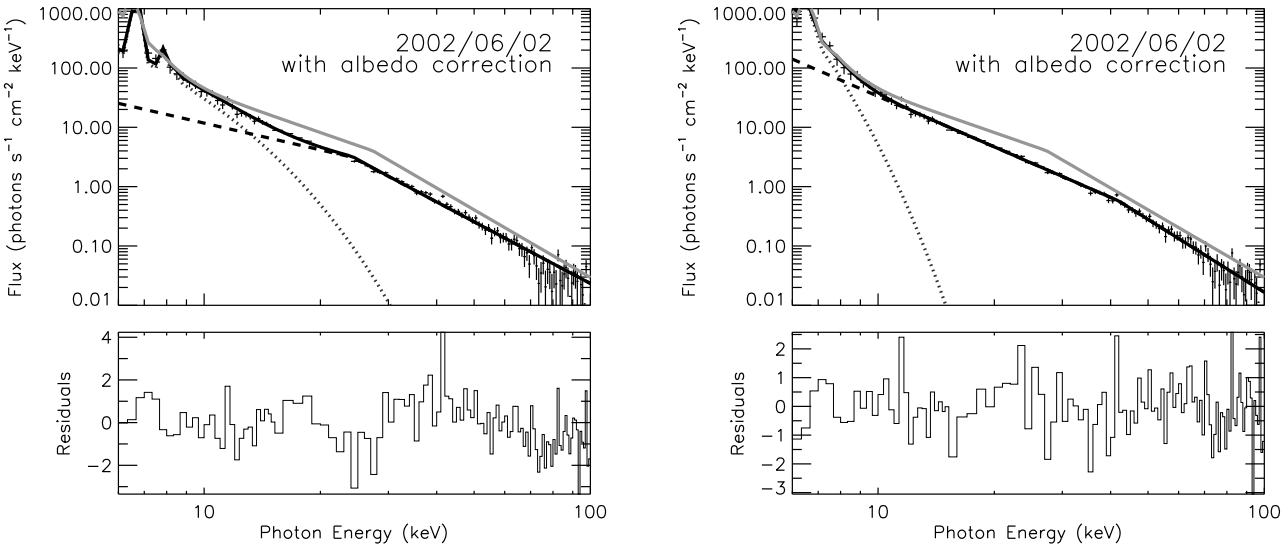

Fig. 6.— Albedo-corrected *RHESSI* spectrum (dark solid lines) at the HXR peak (11:44:28–11:44:32 UT) in the 2002 June 2 flare. The spectrum without albedo correction is overlaid (gray, solid lines). Left panel: The nonthermal part of the spectrum is fitted to single power-law model above ∼21 keV. Right panel: The same spectrum is fitted to a double power-law model with a break energy at ∼40 keV. The (reduced) χ^2 values of the two fits in the left and right panels are 1.4 and 1.0, respectively. The normalized residuals are plotted below each spectrum.

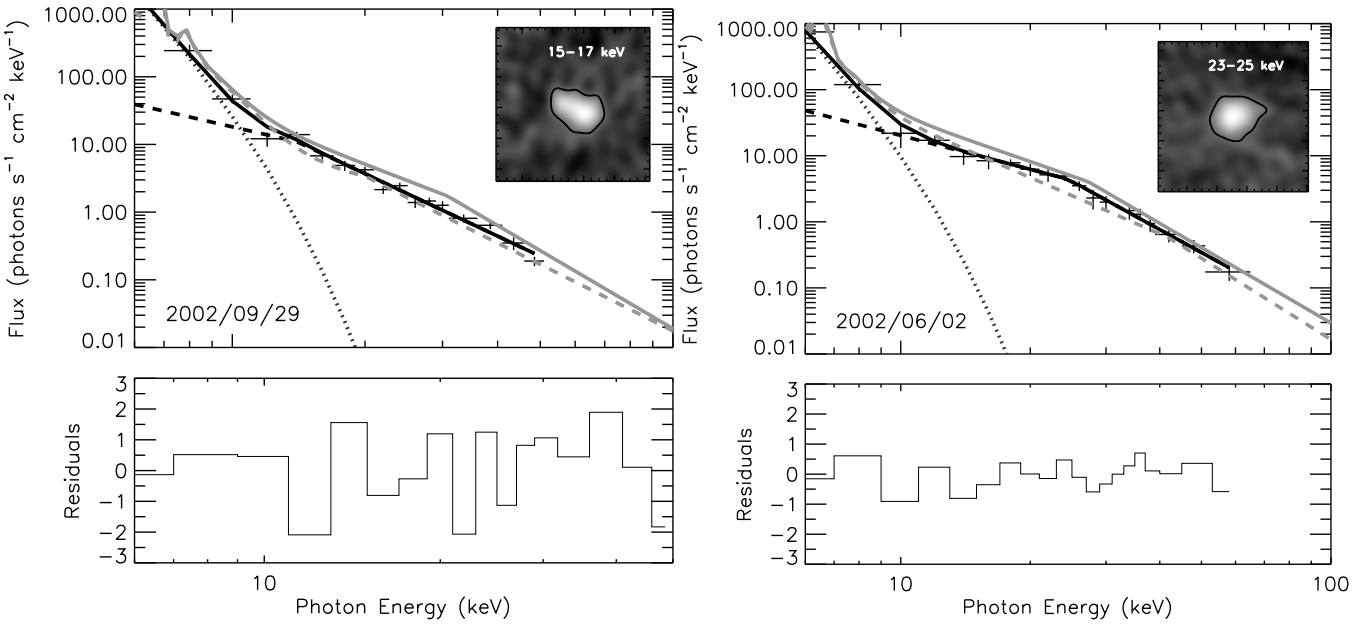

Fig. 7.— Primary source spectra obtained from *RHESSI* images for the September 29, 2002, flare (at 06:35:28 UT, left panel) and the June 02, 2002 flare (at 11:44:28 UT, right panel). The nonthermal part of the spectrum is fitted to single power law function in the left panel and to a double power-law function in the right panel. The solid and dashed gray lines are the fits to the spatially integrated spectra before and after the albedo correction, respectively. The inset in each panel shows one of the *RHESSI* CLEAN images that were used to obtain the spectrum. The contour levels of 30% in the left panel and 28% in the right panel were selected to include only the flux from the primary flare source in each case and to exclude the bulk of the extended albedo source.

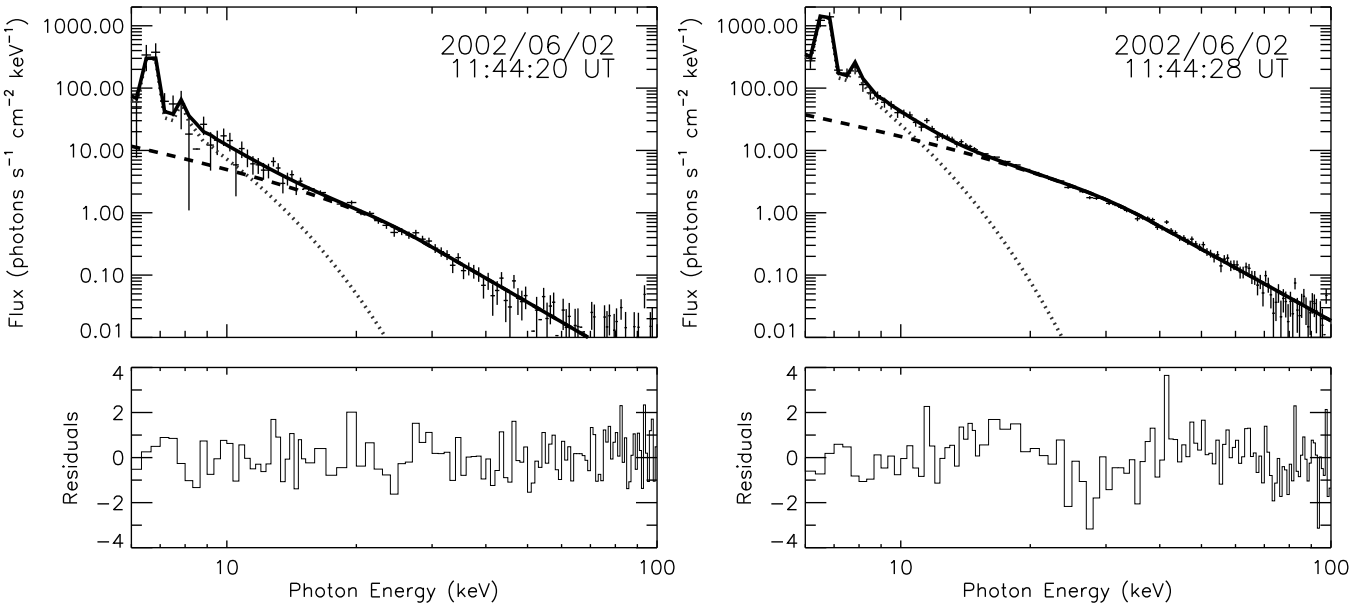

Fig. 8.— Low-energy cutoff interpretation of the nonthermal flattening for two time intervals during the June 2, 2002, flare. In each case, the dashed line shows the best fit to the nonthermal component of a thick-target bremsstrahlung spectrum produced by electrons with a power-law distribution with an index δ and a low-energy cutoff, E_c. The dotted line shows the best fit isothermal bremsstrahlung component to the lower energy X-rays. Normalized residuals are plotted below each spectral fit. Left panel: time interval: 11:44:20 – :24 UT, $\delta = 4.8$, $E_c = 28$ keV. Right panel: time interval: 11:44:28 – :32 UT, $\delta = 4.5$, $E_c = 38$ keV.